



The Microstructure, and Mechanical and Corrosion Properties of As-Cast and As-Extruded Mg-2%Zn-x%Cu Alloys After Solution and Aging Heat Treatments

Changiz Dehghanian, Mehrab Lotfipour, and M. Emamy

(Submitted August 18, 2018; in revised form February 18, 2019; published online March 18, 2019)

The effects of different Cu concentrations and heat treatment on the microstructure, mechanical and corrosion properties of the as-cast and hot-extruded Mg-2%Zn alloys were studied. The results showed that T6 heat treatment led to the dissolution of intermetallics and breaking the continuous networks of intermetallics. Also, the grain size of the base alloy decreased with further Cu additions after solution and aging heat treatments. Microstructural characterization indicated that Mg(Zn,Cu) and Mg(Zn,Cu)₂ intermetallics were formed which their volume fractions increased with exceeding Cu additions. Moreover, the addition of 3 wt.% Cu and T6 heat treatment increased the Brinell hardness of both as-cast and hot-extruded specimens reached to 94 HBN and 116 HBN, respectively. The optimum amounts of the ultimate tensile strength and elongation values obtained from 0.1 wt.% Cu addition for both conditions after T6 treatment which were 253 MPa, 11.5% and 263 MPa, 14.7%, respectively. However, more Cu addition (> 0.5 wt.%) deteriorated the tensile properties of the alloy due to the high volume fraction of intermetallics. The yield tensile strength increased continuously with different Cu additions for the cast and extruded alloys after solution and aging heat treatments. After T6 heat treatment, extruded alloys showed better anti-corrosion properties than those of the cast alloys, while the extruded Mg-2%Zn-0.1%Cu alloy exhibited the best anti-corrosion property. Further Cu addition increased the volume fraction of intermetallics and enhanced the corrosion rate which was due to the galvanic couple effect.

Keywords corrosion behavior, Cu addition, mechanical properties, Mg-2%Zn cast and extruded alloys, microstructural refinement, solution and T6 heat treatments

1. Introduction

Lately, magnesium (Mg) alloys with prolific properties such as low density, lightweight and high specific strength convinced designers to use them in the aerospace and automotive industries. Different properties for Mg alloys are accessible by diverse economical procedures like chemical compositions, plastic deformation and heat treatment (Ref 1). Low-cost Mg-Zn alloys are more effective among other alloys for industrial applications due to the creation of fine precipitates during hot deformation and heat treatment procedures (Ref 2, 3).

Generally, heat treatment process is one of the commercial ways to improve the microstructure and mechanical features for the cast and wrought Mg alloys via precipitation hardening. In this case, shape and distribution of the precipitates during the aging process are the most predominant factors which by controlling them, extraordinary results in mechanical properties will be obtained (Ref 2, 4).

As reported by other researchers (Ref 3, 5, 6), the temperature and time of aging, pre-extrusion and addition of alloying elements have major influences on the features of the

precipitates. Each alloy shows the best properties such as hardness and tensile properties in a particular time and temperature during aging, due to the enhancement of the fine precipitate densities. After that in certain conditions, these properties degrade because of the over-aging phenomenon (Ref 3, 7). Applying extrusion prior to aging treatment introduces more nucleation sites for precipitations than that for unextruded alloys (Ref 6). Besides, alloying elements have a significant effect on the size and distribution of the precipitates (Ref 6, 7).

As discussed before, the Mg-Zn wrought alloys are well known for their heat treatable feature (Ref 2), which their precipitation sequence is (Ref 8, 9):

SSSS (supersaturated solid solution), G.P. zone (Guinier-Preston zone), β'_1 (MgZn₂/Mg₄Zn₇), β'_2 (MgZn₂), β (Mg₂Zn₃/MgZn).

The main precipitates in the system are the rod β'_1 and plate β'_2 , which the rod β'_1 is related to the peak-aged situation and can increase the mechanical properties of the alloy remarkably. However, the plate β'_2 contributes to the over-aged condition, which mechanical properties are deteriorated with its increment (Ref 7). In addition, size and distribution of the rod β'_1 precipitate are the important issues, which can be improved by deformation process and the addition of alloying elements.

According to results obtained from Wang et al. (Ref 10) research, there were more Mg-Zn-containing precipitates formed with aging after extrusion, which deliberately enhanced the tensile properties. Also, Huang et al. (Ref 6) deduced that extrusion before aging resulted in the modification of microstructure and precipitations for Mg-Sn alloy. However, the age-hardening response was not observed much more than the non-extruded alloy due to the dynamic precipitation during the

Changiz Dehghanian, Mehrab Lotfipour, and M. Emamy, University of Tehran, Tehran, Iran. Contact e-mail: cdehghan@ut.ac.ir.

extrusion process. Besides, alloying elements can affect the aging behavior of the alloy from two aspects: accelerating the precipitation nucleation and modifying the precipitation morphology (Ref 2, 7, 9, 11). In the case of Mg-Zn alloys, alloying elements which were added to improve the age-hardening response are Cu (Ref 7, 11), Al (Ref 9), Sn (Ref 10), Ca (Ref 12) and RE (Ref 13). Among these elements, Cu is an effective element for the Mg-Zn systems. According to results obtained from Buha (Ref 2) work, Cu considerably reduced the peak-age time for the Mg-Zn alloy. In addition, by 0.5-1 wt.% Cu addition to the Mg-6%Zn-0.6%Zr alloy, the best form of the rod β_1 precipitates in uniform distribution and high aspect ratio could be achieved. Therefore, this improvement could promote the age-hardening response and raise the UTS and elongation values from 209.4 MPa and 6.1% for Mg-6%Zn-0.6%Zr alloy to 266.3 MPa and 16.1% with 0.5 wt.% Cu addition, respectively. However, more Cu additions can be conducted to the formation of more Cu-rich intermetallics and low number density and aspect ratio of the rod β_1 precipitate, which degraded the age-hardening response of the alloy (Ref 7). According to Zhu et al. (Ref 11), 0.5 wt.% Cu addition to Mg-6%Zn-4%Al alloy and applying double-aging process improved the tensile properties of the alloy by introducing high volume fraction of precipitates.

Likewise, several heat treatment procedures can alter the corrosion resistance of the alloy, due to the dependence of corrosion behavior to the microstructural mutation (Ref 14-17). Generally, the corrosion resistance of Mg alloys relates to second phases, which mostly act as micro-cathode situations and accelerates the corrosion rate (Ref 14). In this case, size, morphology and distribution of the second phases play important roles for determination of the corrosion resistance. Heat treatment can convert features of the second phases for the achievement of finer corrosion properties. According to Song et al. (Ref 14), with the increment of the aging time in the Mg-5%Zn alloy, more volume fraction of the Mg-Zn related to second phases was formed which were led to a worsening of corrosion resistance. In the Mg-2.4%Zn-0.8%Gd alloy, more homogeneous distribution of the lower-size second phases and higher corrosion resistance were caused by the applied solution treatment (Ref 15).

In this investigation, the effect of Cu and T6 heat treatment before and after extrusion on microstructure, tensile and corrosion properties of Mg-2%Zn alloy has been probed.

2. Experimental Procedure

For preparing of the Mg-2%Zn-x%Cu (wt.%) ($x = 0, 0.1, 1$ and 3) alloys, pure Mg, Zn and Cu were used to make the Mg-50%Zn and Mg-20%Cu master alloys via an electric resistance furnace which was aerated with the protection of the CO₂ and SF₆ atmosphere. In the first step, the molten Mg-2%Zn alloy was prepared at 750 °C by the use of Mg-50%Zn master alloy. Furthermore, to make different concentrations of Cu, Mg-20%Cu master alloy was added to the melt with calculated contents. Eventually, after holding the melts at 750 °C for 5 min, they were poured into a steel mold, preheated to 250 °C, to produce the cylindrical ingots with the diameter of 34 mm and the length of 45 mm.

Then, the Mg-2%Zn and Cu-containing alloys, in as-cast condition, were homogenized at 315 °C and 435 °C, respectively, for 48 h followed by water quenching. After that, they were solutionized at 315 and 435 °C, respectively, for 5 h followed by water quenching (Ref 2). For age hardening of the cast samples, some billets were subjected to heat treatment at 160 °C for 16 h (Ref 2).

For extrusion process, the machined cast specimens were preheated up to 300 °C for 1 h in an electrical resistance furnace and then pressed with a ram speed of 1 mm/s with an extension ratio of 12:1. Afterward, extruded samples of the Mg-2%Zn and Mg-2%Zn-Cu-bearing alloys were solutionized at 315 and 435 °C, respectively, for 5 h followed by water quenching, then aged at 140 °C for 16 h. Figure 1 schematically presents the heat treatment cycles for the cast and extruded alloys.

The temperature for the extruded alloys was lower than that of the cast alloys due to more precipitation formation after the extrusion process. In addition, for microstructural observations, all samples were ground and etched by acetic-picric solution (5 ml acetic acid + 6 g picric acid + 10 ml H₂O + 100 ml ethanol) (Ref 18). Lately, the surface of samples was analyzed by the optical microscopy (OM) and scanning electron microscopy (SEM) which SEM was done by performing in the Vega©Tescan microscope equipped with energy dispersive spectroscopy (EDS) system. Besides, phase exploration was conducted by the Philips binary diffractometer with Cu-k α radiation.

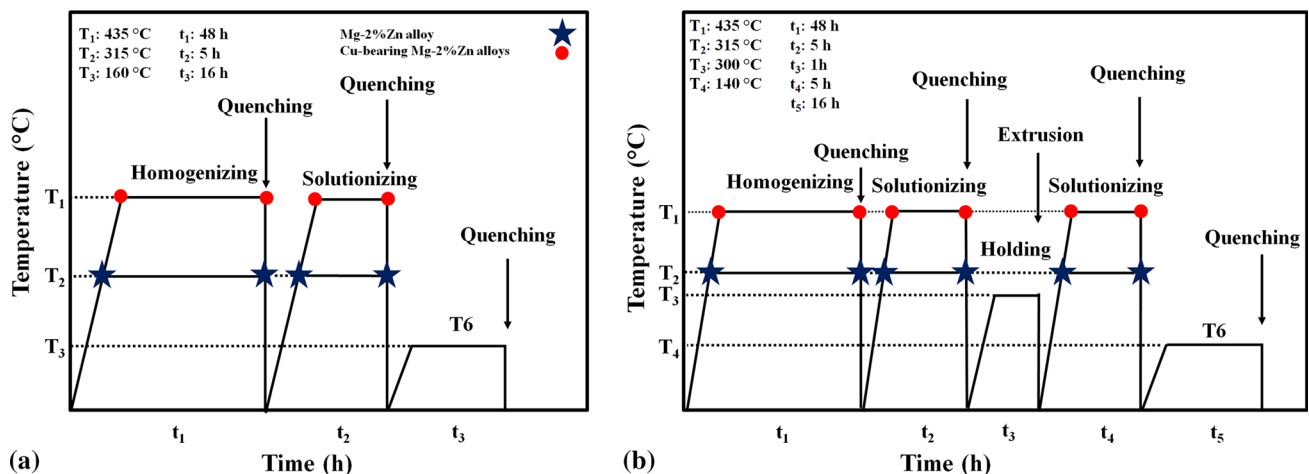


Fig. 1 Heat treatment cycles for the (a) cast and (b) extruded Mg-2%Zn and Cu-bearing Mg-2%Zn alloys

For ambient tensile properties, the heat-treated cast and extruded samples were machined according to ASTM: E8/E8M-16a and then stretched with a computerized testing machine (SANTAM STM-20) at the constant crosshead speed of 1 mm/min at room temperature. The fracture surfaces of the tensile test specimens were also examined with the same SEM equipment.

To obtain the polarization and electrochemical impedance spectroscopy (EIS) results, eight samples (i.e., aged cast and extruded samples) were prepared with the surface area of 100 mm² used as a working electrode. Two other electrodes which were a platinum plate anode and the saturated calomel were utilized to set a three-electrode cell system in 3.5 wt.% NaCl solution. The measurements were started at -200 mV with respect to open circuit potential (OCP) state after suspension of the system for 300 s to reach a stable potential. Afterward, the voltage increased with 1 mV S⁻¹ interval up to the point that the final current density reaches 10 mA/cm². By a mathematical extrapolation called Tafel region, the corrosion current density (I_{corr}) and corrosion potential (E_{corr}) were obtained from the polarization curves. EIS measurements were performed at the frequency ranged from 100 kHz to 0.1 Hz with a voltage amplitude of 10 mV. The EIS spectra were fitted with an equivalent circuit using the Zview software.

3. Results and Discussion

Figure 2 displays the optical micrographs of the cast and extruded Mg-2%Zn-x%Cu alloys after solutionizing heat treatment.

By considering to our later investigation on the cast Mg-2%Zn alloy and also other related research work (Ref 18, 19), the cast alloys consisted of the α -Mg phase and two main intermetallics: MgZnCu (in the form of small particles) and Mg(Zn,Cu)₂ (in the form of large particles) phases were distributed along the grain boundaries. Moreover, increasing the Cu contents created a continuous network from intermetallics around the dendrite boundaries (Ref 19). From Fig. 2, the microstructures of the alloys with 0 and 0.1 wt.% Cu

contents consist of grain boundaries with minor quantities of second-phase particles. However, with more Cu additions, the volume fraction of second-phase particles increased significantly. In addition, in comparison with the same cast alloys (Ref 19), the solution treatment was led to the incomplete dissolution of the intermetallics into the α -Mg matrix and breakage of the continuous networks of second phases [i.e., MgZnCu and Mg(Zn, Cu)₂] to the separated particles (as seen with white arrows). Figure 2(e) and (f) shows the OM micrographs of extruded alloys after solution treatment from the transversal section of the extruded samples. Accordingly, a fine grain structure has been formed after applying the hot extrusion. Besides, second-phase particles have been broken and dispersed along the extrusion direction, acting as appropriate sites for recrystallized grains and also for precipitations nucleation (Ref 6). In addition, with more Cu additions, microstructures indicated a decrement tendency in grain size. From Fig. 2(e) and (f), it can be deduced that with solution heat treatment some grains tend to grow, due to the applied high-temperature heat treatment.

Figure 3 illustrates the optical micrographs of the cast and extruded Mg-2%Zn-x%Cu alloys after T6 heat treatment.

As can be seen, the microstructures of the cast and extruded alloys were identical to the same alloys after solutionizing heat treatment. In this case, as depicted in Fig. 3(a), (b), (e) and (f), the microstructures of the cast and extruded Mg-2%Zn and Mg-2%Zn-0.1%Cu alloys nearly presented the α -Mg matrix and some grain boundaries with no sign of intermetallics. But, the volume fraction and size of the particles enhanced for alloys with higher Cu contents.

Figure 4 presents the SEM micrographs of the cast Mg-2%Zn-x%Cu alloys after T6 heat treatment.

Figure 4(e), (f), (g) and (h) presents the higher SEM magnification from the chosen section of Fig. 4(d) and also related map EDS analysis. As can be understood, the distributed particles have been mainly consisted of Mg, Cu and Zn elements. Besides, point EDS analysis from some small and big bright particles is listed in Table 1. For the large and bulky particles marked as A, the average chemical composition has been related to Mg(Zn, Cu)₂ compounds. Also, for small

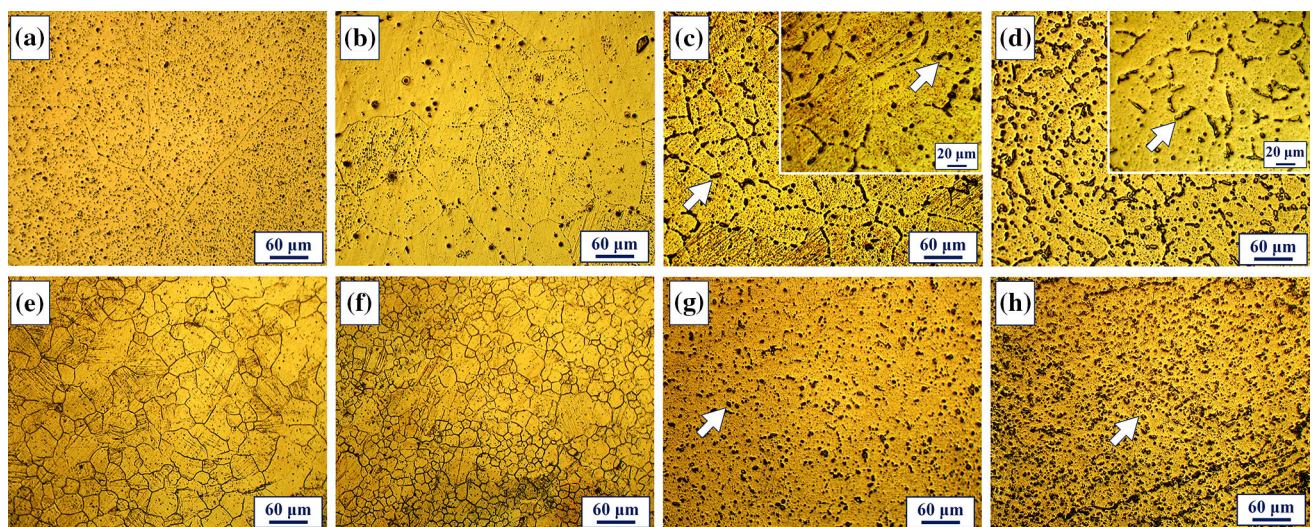


Fig. 2 Optical micrographs after solution treatment; for the cast (a) Mg-2%Zn, (b) Mg-2%Zn-0.1%Cu, (c) Mg-2%Zn-1%Cu and (d) Mg-2%Zn-3%Cu alloys and also for the extruded (e) Mg-2%Zn, (f) Mg-2%Zn-0.1%Cu, (g) Mg-2%Zn-1%Cu and (h) Mg-2%Zn-3%Cu

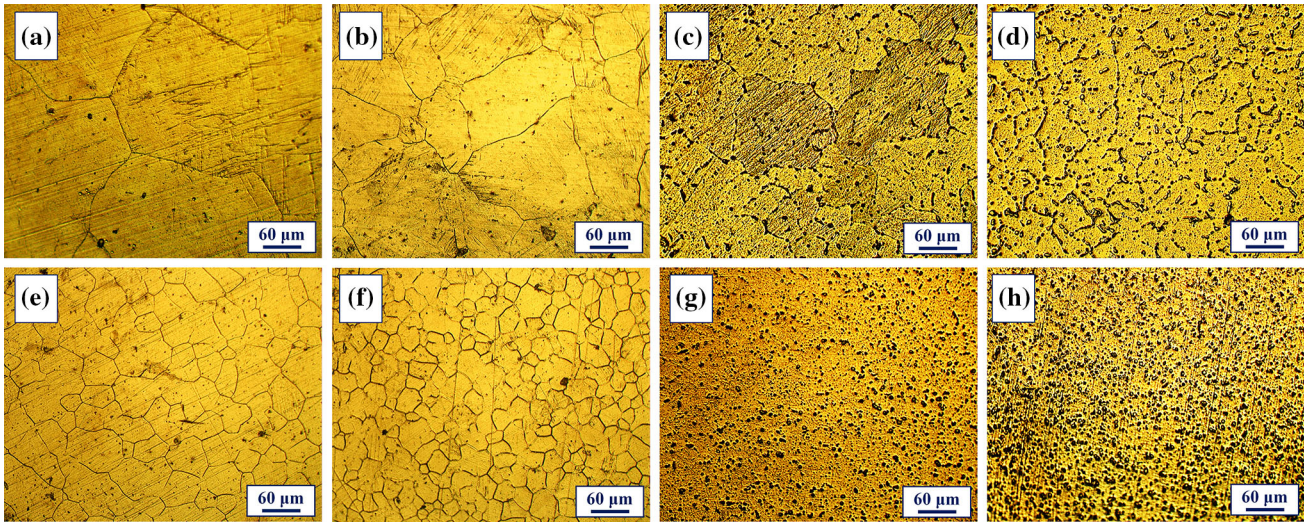


Fig. 3 Optical micrographs after aging heat treatment; for the cast (a) Mg-2%Zn, (b) Mg-2%Zn-0.1%Cu, (c) Mg-2%Zn-1%Cu and (d) Mg-2%Zn-3%Cu alloys and also for the extruded (e) Mg-2%Zn, (f) Mg-2%Zn-0.1%Cu, (g) Mg-2%Zn-1%Cu and (h) Mg-2%Zn-3%Cu

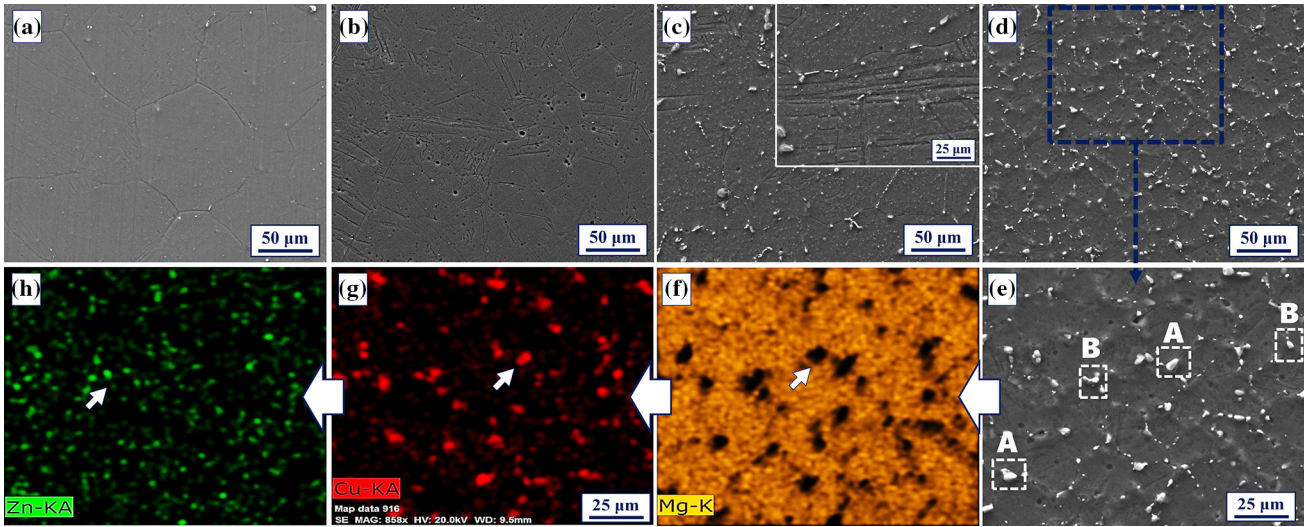


Fig. 4 SEM micrographs after T6 heat treatment; for the cast (a) Mg-2%Zn, (b) Mg-2%Zn-0.1%Cu, (c) Mg-2%Zn-1%Cu and (d) Mg-2%Zn-3%Cu alloys and also (e), (f), (g) and (h) EDS map analysis from the area of the Mg-2%Zn-3%Cu alloy

Table 1 EDS point analysis quantities from the marked points of Fig. 4(e) and 5(d)

	Marking point	Element	at. %
Figure 4(e)	A	Mg	34.26
		Zn	11.09
		Cu	54.65
	B	Mg	79.10
		Zn	6.47
		Cu	14.43
Figure 5(d)	C	Mg	31.83
		Zn	8.21
		Cu	59.96
	D	Mg	74.50
		Zn	2.28
		Cu	23.22

particles marked as B, the average chemical composition has been contributed to MgZnCu intermetallics.

Figure 5(a), (b), (c) and (d) clarifies the SEM micrographs for the extruded Mg-2%Zn-x%Cu alloys after T6 heat treatment.

The microstructures demonstrate fine grains and second-phase particles which their volume fraction enhanced with the improvement of the Cu contents. For more analysis, grain size and volume fraction of the extruded alloys after solution and T6 heat treatments are calculated and tabulated in Table 2.

As can be realized from Table 2, for the solutionized extruded Mg-2%Zn alloy, grain size was found to be 38 μm which with 3 wt.% Cu addition reduced to about 11 μm. However, the aged extruded Mg-2%Zn alloy had the grain size about 60 μm which with 3 wt.% Cu, the grain size of the alloy decreased to about 28 μm. Furthermore, with the increment of the Cu content from 0 to 3 wt.%, the volume fraction of

Table 2 Values for the average grain size and volume fraction of intermetallics for the extruded Mg-2%Zn-x%Cu after solution and T6 treatments

Solution heat treatment	Mg-2%Zn	Mg-2%Zn-0.1%Cu	Mg-2%Zn-1%Cu	Mg-2%Zn-3%Cu
Grain size, μm	38 ± 13	20 ± 7	14 ± 7	11 ± 5
Volume fraction	~ 0	~ 0	6.7	13.6
T6 heat treatment	Mg-2%Zn	Mg-2%Zn-0.1%Cu	Mg-2%Zn-1%Cu	Mg-2%Zn-3%Cu
Grain size, μm	60 ± 15	47 ± 11	34 ± 12	28 ± 9
Volume fraction	~ 0	~ 0	5.3	12.8

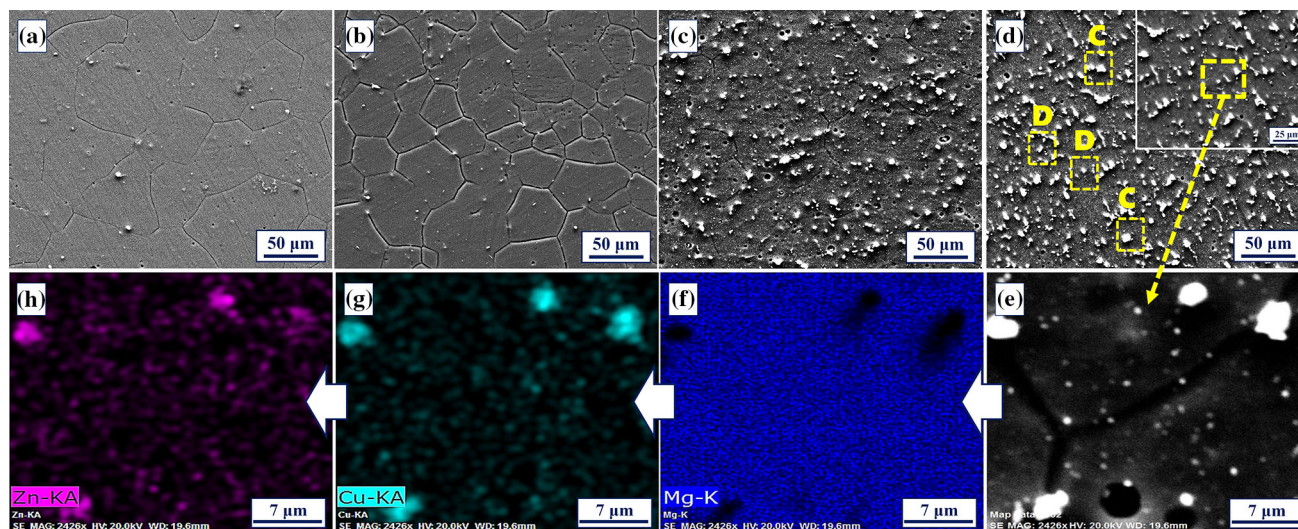


Fig. 5 SEM micrographs after T6 heat treatment; for the extruded (a) Mg-2%Zn, (b) Mg-2%Zn-0.1%Cu, (c) Mg-2%Zn-1%Cu and (d) Mg-2%Zn-3%Cu alloys and also (e), (f), (g) and (h) EDS map analysis from the area of the Mg-2%Zn-3%Cu alloy

second-phase particles for the extruded alloys was reduced from about 0 to 13.6% (after the solutionizing) and also 0 to 12.8% (after T6 heat treatment), respectively. With respect to the variation of grain size and the volume fraction values, slight grain growth and dissolution of intermetallics were observed in the matrix after applying T6 heat treatment. Figure 5(e), (f), (g) and (h) presents the magnified SEM micrographs from the determined section of the extruded Mg-2%Zn-3%Cu alloy and also related elemental maps of EDS analysis. As can be observed, three particles have been distributed along the grain boundaries which mainly consisted of the Mg, Zn and Cu elements. As a further matter, from Table 1, the average chemical compositions have been calculated by point EDS analysis from two different morphologies; big and bulky particles marked as C and small particles marked as D, clarified that big and bulky particles were $\text{Mg}(\text{Zn,Cu})_2$ phases and small particles were MgZnCu intermetallics.

To describe the effect of heat treatment on the phase constituents, the alloys were examined with the XRD analysis as shown in Fig. 6.

As can be noticed, the main phases for the cast and extruded Mg-2%Zn-1%Cu and Mg-2%Zn-3%Cu alloys after the solution and T6 heat treatments are the α -Mg, MgZnCu and $\text{Mg}(\text{Zn,Cu})_2$ phases, that confirmed the microstructural observations. Besides, with the higher Cu addition, Mg-related peak intensities reduced and new $\text{Mg}(\text{Zn,Cu})_2$ -related peaks ob-

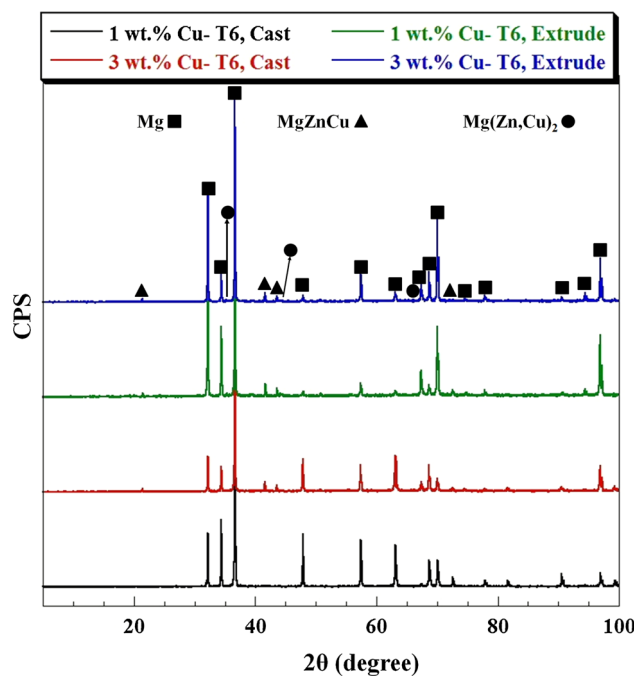


Fig. 6 XRD patterns after T6 heat treatment; for the cast (a) Mg-2%Zn-1%Cu and (b) Mg-2%Zn-3%Cu and the extruded (c) Mg-2%Zn-1%Cu and (d) Mg-2%Zn-3%Cu alloys

served with specific degrees. Comparison between cast and extruded specimens revealed that Mg-related peaks have been intensified more for the extruded alloys due to more dissolution of the second phases into the matrix.

3.1 Mechanical Properties

Table 3 displays the mechanical properties of the cast and extruded Mg-2%Zn-x%Cu alloys after solutionizing and T6 heat treatments.

Figure 7 shows the Brinell hardness variation with different Cu contents in two conditions (solution and age heat treatment) for the cast and extruded alloy. Hardness is measured on the transversal plane for the extruded samples.

Hardness value for the cast Mg-2%Zn alloy after solution heat treatment is about 59 BHN, which with aging treatment increased to 75 BHN. On the other hand, the extrusion process together with the solution treatment appropriately enhanced the hardness value to about 85 BHN, which after aging reached 88 BHN. Enhancement of the Cu content to 3 wt.%, properly increased the hardness value to 82 BHN for the cast alloy and 110 BHN for the extruded alloy with the solution heat treatment. Moreover, the aging treatment improved the hardness to 94 BHN for the cast alloys and 116 BHN for the extruded alloy. Consequently, hardness values increased due to three main reasons: first, enrichment of the secondary precipitates after the heat treatment for both cast and extruded alloys. Second, for the extruded samples; mechanical working helps to an enhancement of the hardness values, and also the third reason is increasing of the Zn, Cu-containing second-phase intermetallics with more the Cu contents.

Figure 8 presents the tensile properties of the cast and extruded alloys in two solution and cast conditions.

It can be extinguished that with 0.1 wt.% Cu addition to the cast and extruded alloys, the best properties were obtained in both solution and age conditions. Moreover, the extruded alloys exhibited better characteristics than the cast alloys. When the Cu content exceeded from 0.1 to 3 wt.% Cu, the UTS and elongation values declined. With solution treatment, the UTS and elongation values achieved 202 MPa, 10.6% for the cast and 239 MPa, 14.1% for the extruded Mg-2%Zn alloy, respectively. In addition, with 0.1 wt.% Cu addition, these

values raised to 235 MPa, 11.1% and 255 MPa, 15.2%, respectively. However, with 3 wt.% Cu addition, the UTS and elongation values decreased to some extent as 191 MPa, 9.7% and 249 MPa, 11.9%, respectively. On the other hand, a remarkable increment of the UTS values and decrement of the elongation values achieved after aging treatment. The typical stress–strain curves of the cast and extruded Mg-2%Zn-x%Cu ($x = 0, 0.1$ and 3) alloys after the aging treatment are shown in Fig. 9.

After aging treatment, the UTS and elongation values changed to 215 MPa, 9.4% for the cast and 249 MPa, 13.2% for the extruded Mg-2%Zn alloy, separately. Compared to the Mg-2%Zn, 0.1 wt.% Cu addition could effectively alter the UTS and elongation values to 253 MPa, 10.5% and 263 MPa, 14.7%, respectively, for the cast and extruded alloys. However,

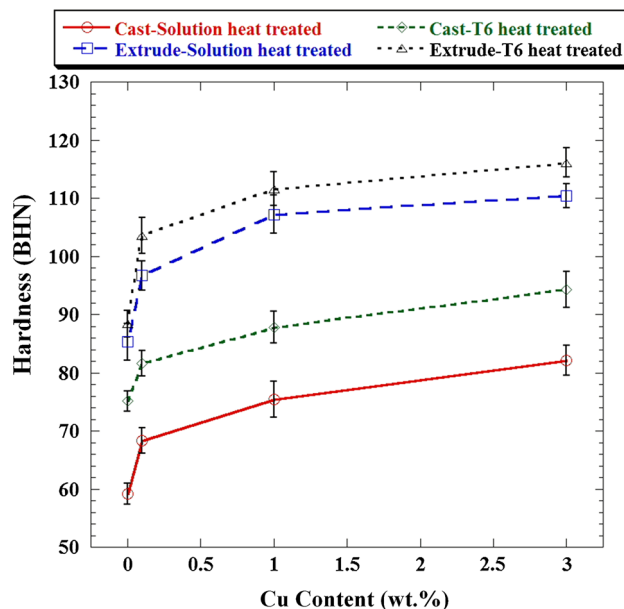


Fig. 7 Brinell hardness of the cast and extruded Mg-2%Zn-x%Cu alloys after solution and T6 treatments as a function of copper concentration

Table 3 Mechanical properties of the cast and extruded Mg-2%Zn-x%Cu alloys after solution and T6 treatments

Process	Alloy	Ultimate tensile strength (UTS), MPa	Tensile elongation, %	Yield tensile strength (YTS), MPa	Brinell hardness (HBN)
Cast + solution	Mg-2%Zn	202 ± 5	10.6 ± 0.3	95 ± 2	59 ± 2
	Mg-2%Zn-0.1%Cu	235 ± 4	11.1 ± 0.3	105 ± 3	68 ± 2
	Mg-2%Zn-1%Cu	223 ± 6	10.8 ± 0.4	112 ± 3	75 ± 3
	Mg-2%Zn-3%Cu	191 ± 9	9.7 ± 0.3	121 ± 3	82 ± 3
Cast + T6	Mg-2%Zn	215 ± 6	9.4 ± 0.2	119 ± 4	75 ± 2
	Mg-2%Zn-0.1%Cu	253 ± 4	10.5 ± 0.2	130 ± 3	82 ± 2
	Mg-2%Zn-1%Cu	246 ± 5	9.6 ± 0.3	138 ± 4	88 ± 3
	Mg-2%Zn-3%Cu	210 ± 6	8.4 ± 0.2	143 ± 2	94 ± 3
Extrude + solution	Mg-2%Zn	239 ± 6	14.1 ± 0.3	131 ± 3	85 ± 3
	Mg-2%Zn-0.1%Cu	255 ± 6	15.2 ± 0.4	149 ± 3	97 ± 2
	Mg-2%Zn + 1%Cu	251 ± 5	13.7 ± 0.2	164 ± 5	107 ± 3
	Mg-2%Zn-3%Cu	249 ± 5	11.9 ± 0.3	175 ± 3	110 ± 3
Extrude + T6	Mg-2%Zn	249 ± 5	13.2 ± 0.2	191 ± 5	88 ± 2
	Mg-2%Zn-0.1%Cu	263 ± 6	14.7 ± 0.2	211 ± 3	104 ± 3
	Mg-2%Zn-1%Cu	258 ± 5	14.1 ± 0.3	218 ± 4	112 ± 3
	Mg-2%Zn-3%Cu	254 ± 7	10.3 ± 0.4	224 ± 4	116 ± 2

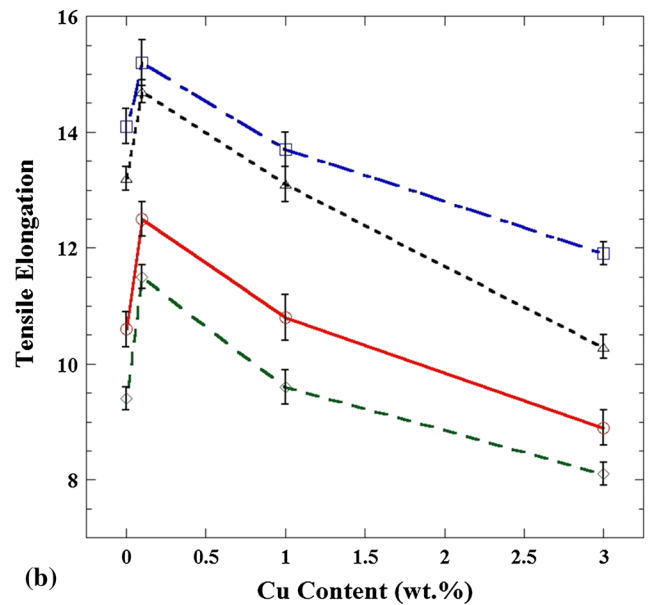
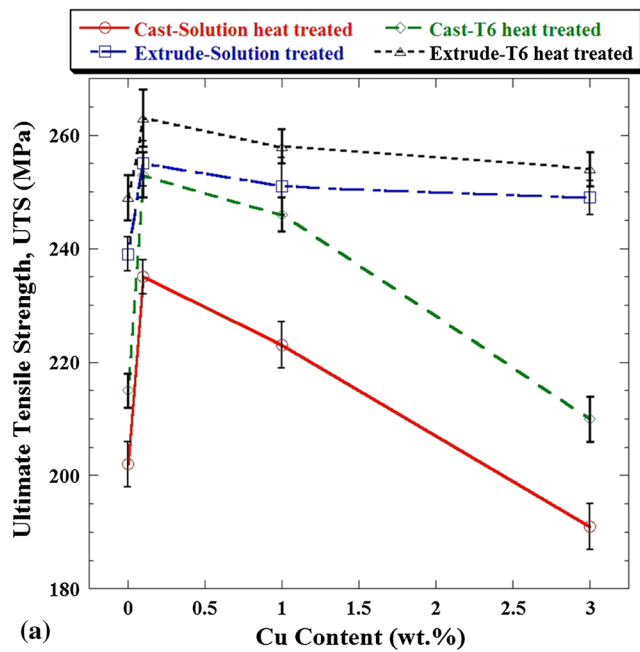


Fig. 8 Variation of the UTS, and tensile elongation for the cast and extruded Mg-2%Zn-x%Cu alloys after solution and T6 treatments percent as a function of Cu concentration

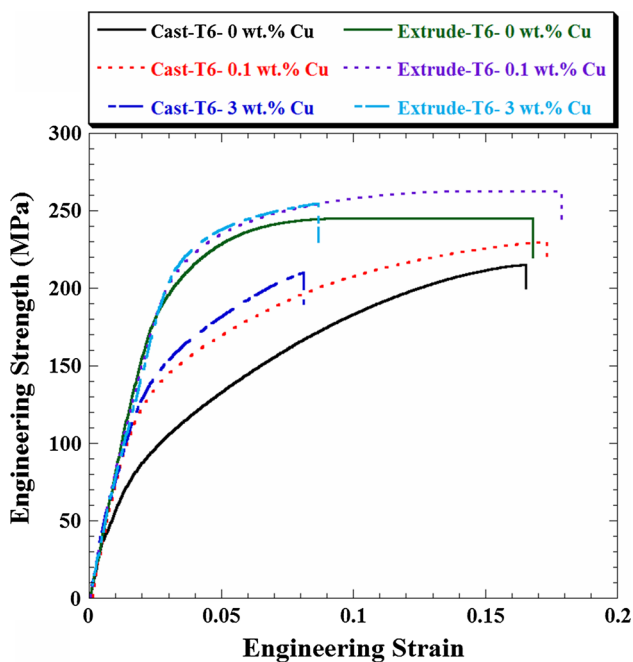


Fig. 9 Engineering stress vs. engineering elongation as a function of Cu concentration after T6 heat treatment

the tensile values reduced with 3 wt.% Cu addition to 210 MPa, 8.4% and 254 MPa, 10.3%, relatively. Moreover, tensile strength (YTS) was increased continuously with different Cu additions for the cast and extruded alloys after solution and aging heat treatments. Clearly, the extruded alloys showed greater yield strength than that of the cast alloys. The YTS values were higher after the aging heat treatment which was higher in comparison with the solution heat treatment.

According to Zhu et al. (Ref 11), grain refinement due to Cu additions and also precipitation strengthening were main factors in the improvement of the tensile properties for the Mg-6%Zn-4%Al alloy after aging treatment. Based on our previous investigation (Ref 19), 0.1 wt.% Cu addition properly enhanced the cast tensile properties. However, higher Cu additions deteriorated the properties due to the high volume fraction of semi-continuous network of second-phase particles (Ref 19). It should be noted that with solution heat treatment, intermetallics lightly dissolved into the matrix and network structure of intermetallics broken. At the same time, the shape of the particles altered to more round-like. Nevertheless, reducing the crack initiation sources and improving the UTS values for the cast alloys could be caused by these three mentioned factors. Conversely, elongation for the aged cast alloys declined in comparison with that of the solutionized cast alloys, which generally could be related to the precipitation hardening (Ref 20).

Generally, after hot extrusion, the finer microstructure with higher tensile properties compared to the cast condition achieved. Therefore, after solution heat treatment, extruded samples showed greater tensile values than the cast samples. Similar to the cast alloys, aging treatment could be led to an improvement of the UTS values and reduction in the elongation values for extruded alloys. As a result, with 0.1 wt.% Cu, an optimum level of the UTS and elongation values obtained and 3 wt.% Cu contributes a high volume fraction of the second-phase particles which ruins the tensile properties. Consequently, fine tensile properties of extruded alloys related to lower grain size, grain boundary strengthening, higher dissolution of the intermetallics into the matrix, breakage the network structure of the second phases, homogenous distribution of them and also precipitation hardening (Ref 20). However, the increment of the UTS and YTS values from the solution treatment to the aging treatment was higher for the cast alloys, which could be

inferred to the better response of the Mg-Zn-Cu alloys in cast conditions.

Figure 10 presents the tensile fracture surface of the cast and extruded alloys after T6 heat treatment shown with SEM.

As can be seen in Fig. 10(a) and (e), cast and extruded Mg-2%Zn alloys after the T6 treatment manifested a cleavage fracture with some tearing ridges and the small ductile area as shown in Fig. 10(a) and (e). By considering to other Cu-containing alloys, the cast and extruded Mg-2%Zn-0.1, 1 and 3%Cu alloys demonstrated a semi-cleavage and semi-ductile fractures with a lot of dimples in their surfaces. Apparently, the dimples were bigger and deeper for extruded alloys than cast alloys, which asserted more ductility deterioration in cast alloys. It is interesting to say that some dimples elongated and such river pattern-like model formed for each alloy. On the

other hand, several broken particles have been observed in Cu-containing alloys which their volume fraction and size increased with higher Cu contents. These particles have been recognized as a dominant factor for deterioration of the ductility. Furthermore, these particles have been seen with more volume fraction in the cast Mg-2%Zn-3%Cu alloy in comparison with the same extruded alloy, which designated the dissolution of more intermetallics by the extrusion alongside with the heat treatment.

3.2 Corrosion Behavior

Figure 11 shows the polarization curves for the cast and extruded Mg-2%Zn-x%Cu alloys after T6 heat treatment which was measured in 3.5% NaCl solution.

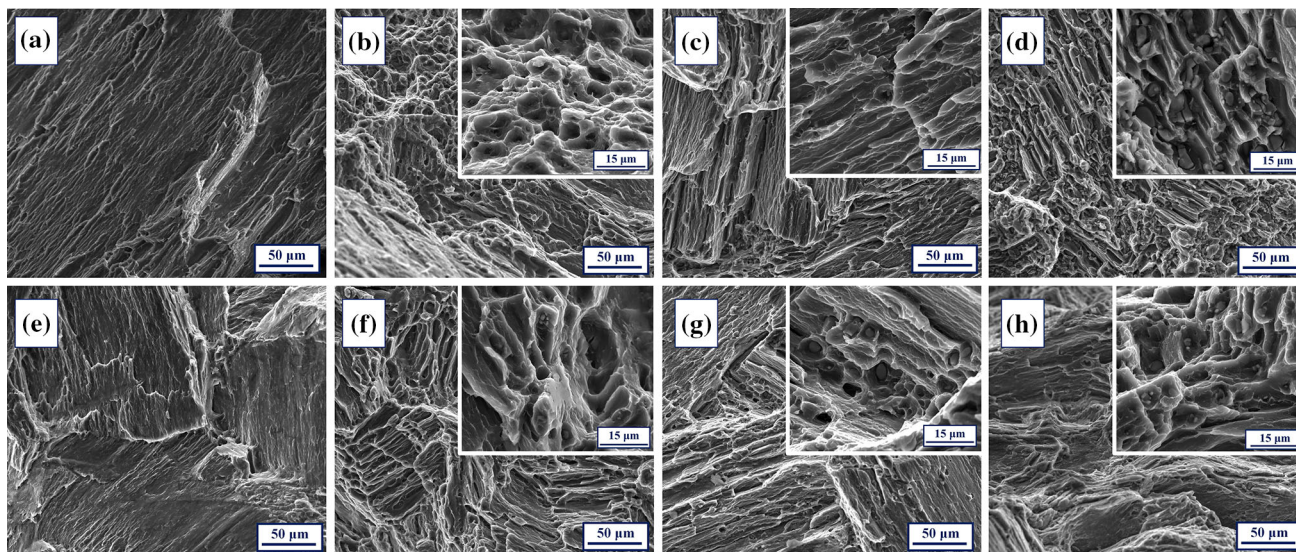


Fig. 10 Fracture surface (SEM micrographs) after T6 heat treatment for the cast Mg-2%Zn alloy with (a) 0 wt.%, (b) 0.1 wt.%, (c) 1 wt.%, (d) 3 wt.%, also for the extruded Mg-2%Zn alloy with (e) 0 wt.%, (f) 0.1 wt.%, (g) 1 wt.%, (h) 3 wt.%

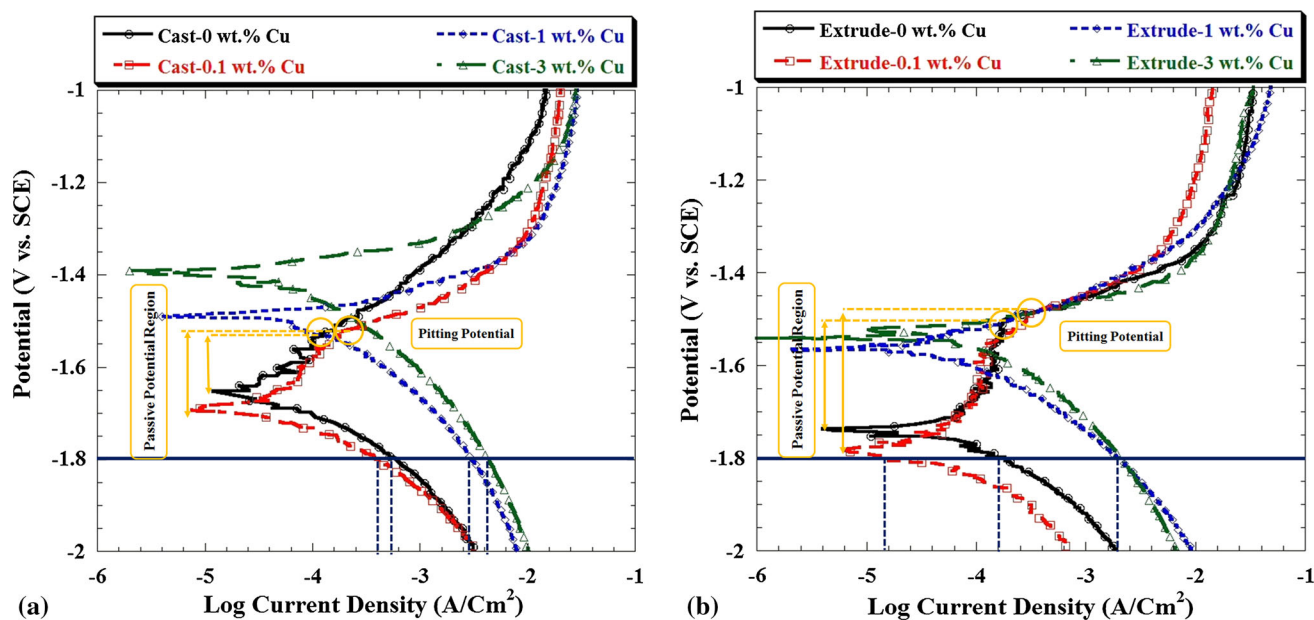


Fig. 11 Polarization curves of (a) the cast and (b) the extruded Mg-2%Zn-x%Cu alloys after T6 heat treatment in 3.5 wt.% NaCl

As can be noticed, the polarization curves consisted of two anodic and cathodic branches, which indicate typical polarization curves. Generally, the cathodic branches occur due to the oxygen evolution reaction, and the anodic branches assert the passivation-like area and existence of the protective films (Ref 21). According to Fig. 11(a) and (b), at a constant potential (-1.8 V), two lines passed from the cathodic regions of polarization curves separately for both cast and extruded alloys. The current density values were estimated as 4.7×10^{-5} , 2×10^{-5} , 1×10^{-4} and 5×10^{-4} (A cm^{-2}) for the cast Mg-2%Zn, Mg-2%Zn-0.1%Cu, Mg-2%Zn-1%Cu and Mg-2%Zn-3%Cu alloys, respectively. Also, for the extruded Mg-2%Zn, Mg-2%Zn-0.1%Cu, Mg-2%Zn-1%Cu and Mg-2%Zn-3%Cu alloys these values were obtained to be 3.7×10^{-5} , 1.5×10^{-5} , 0.5×10^{-4} and 4×10^{-4} (A cm^{-2}), respectively.

Consequently, it can be resulted from these values, the cast and extruded Mg-2%Zn-0.1%Cu alloys showed the lowest current densities which presented the higher corrosion resistance. Conversely, the cast and extruded Mg-2%Zn-3%Cu alloys had the highest current densities. Afterward, E_{corr} and I_{corr} have been calculated directly from the polarization curves by considering the Tafel extrapolation and listed in Table 4.

With respect to Table 4, for the aged cast alloys, the corrosion current density reduced from 4.7×10^{-5} A cm^{-2} for the Mg-2%Zn alloy to 2×10^{-5} A cm^{-2} for the Mg-2%Zn-0.1%Cu alloy. However, it increased with further Cu additions to 5×10^{-4} A cm^{-2} for the Mg-2%Zn-3%Cu alloy. Similarly, for the aged extruded alloys, the corrosion current density for the Mg-2%Zn alloy was calculated to be 3.7×10^{-5} A cm^{-2}

Table 4 Values measured from the polarization curves of the cast and extruded Mg-2%Zn-x%Cu alloys after T6 treatment

Condition	Alloy, wt.%	E_{corr} (V_{SCE})	I_{corr} A cm^{-2}
Cast + T6	Mg-2%Zn	-1.66	4.7×10^{-5}
	Mg-2%Zn-0.1%Cu	-1.69	2×10^{-5}
	Mg-2%Zn-1%Cu	-1.49	1×10^{-4}
	Mg-2%Zn-3%Cu	-1.41	5×10^{-4}
Extrude + T6	Mg-2%Zn	-1.54	3.7×10^{-5}
	Mg-2%Zn-0.1%Cu	-1.78	1.5×10^{-5}
	Mg-2%Zn-1%Cu	-1.56	0.5×10^{-4}
	Mg-2%Zn-3%Cu	-1.54	4×10^{-4}

which was much lower than the I_{corr} for cast Mg-2%Zn alloy. With 0.1 wt.% Cu addition, the I_{corr} value was reached to 1.5×10^{-5} A cm^{-2} which then with the addition of 3 wt.% Cu, its value exceeded to 4×10^{-4} A cm^{-2} .

As can be seen in Fig. 11, from the anodic branches of the polarization curves, the passive potential regions have been observed for the cast and extruded Mg-2%Zn and Mg-2%Zn-0.1%Cu alloys. According to Fig. 11, the pitting potential values for the aged cast Mg-2%Zn and Mg-2%Zn-0.1%Cu alloys were interpreted as -1.53 and -1.51 , respectively. Also, for the aged extruded Mg-2%Zn and Mg-2%Zn-0.1%Cu alloys, these values have been calculated as -1.49 and -1.47 , respectively. On the other hand, the ranges of passive potential region are achieved from Fig. 11 as 0.12 (for cast Mg-2%Zn), 0.19 (for cast Mg-2%Zn-0.1%Cu), 0.25 (for extruded Mg-2%Zn) and 0.31 (for extruded Mg-2%Zn-0.1%Cu) (V). As can be deduced, extruded alloys had more positive pitting potential and also higher ranges of the passive potential region, which represented the formation of more stable films on the extruded alloys. Also, the Mg-2%Zn-0.1%Cu extruded alloy had the best corrosion resistance as obtained from polarization curves results. Figure 12 and 13 manifests the EIS curves for the cast and extruded Mg-2%Zn-x%Cu alloys after T6 heat treatment, respectively, which were measured in 3.5% NaCl solution.

The Nyquist spectra for the cast Mg-2%Zn alloy presented two capacitance loops at high and medium frequencies. Nevertheless, for other cast and extruded alloys, one low-frequency inductance loop was formed in addition to the two other loops. Additionally, the diameter of the loops for the cast and extruded alloys decreased with the following sequences: Mg-2%Zn-0.1%Cu, Mg-2%Zn, Mg-2%Zn-1%Cu and Mg-2%Zn-3%Cu, which the extruded alloys had greater loops than that of the cast alloys. The Bode plot of $|Z|$ versus frequency (Fig. 12b and 13b) and the phase angle plot versus frequency (Fig. 12c and 13c) showed the same characteristics as they were observed in the Nyquist spectra for the cast and extruded alloys. To analyze the EIS curves more deeply, electrochemical equivalent circuit models have been utilized according to Ref 21, to fit the EIS data and the kinetic parameters are calculated and listed in Table 5.

The parameters, respectively, named as R_s : solution resistance, C , and R_{ct} : high-frequency capacitance and resistance, R_f and C_f : film resistance and film capacitance, related to the film formation on the surface of the samples, and the last part w

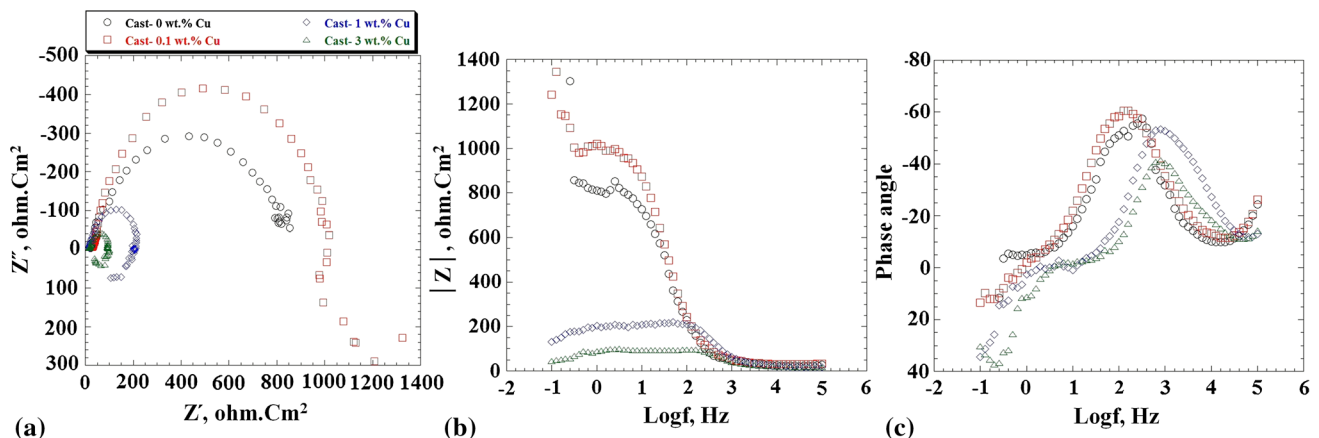


Fig. 12 EIS spectra of the cast Mg-2%Zn-x%Cu alloys in 3.5 wt.% NaCl solution: (a) Nyquist plots; (b) Bode plots of $|Z|$ vs. frequency and (c) Bode plots of degree vs. frequency

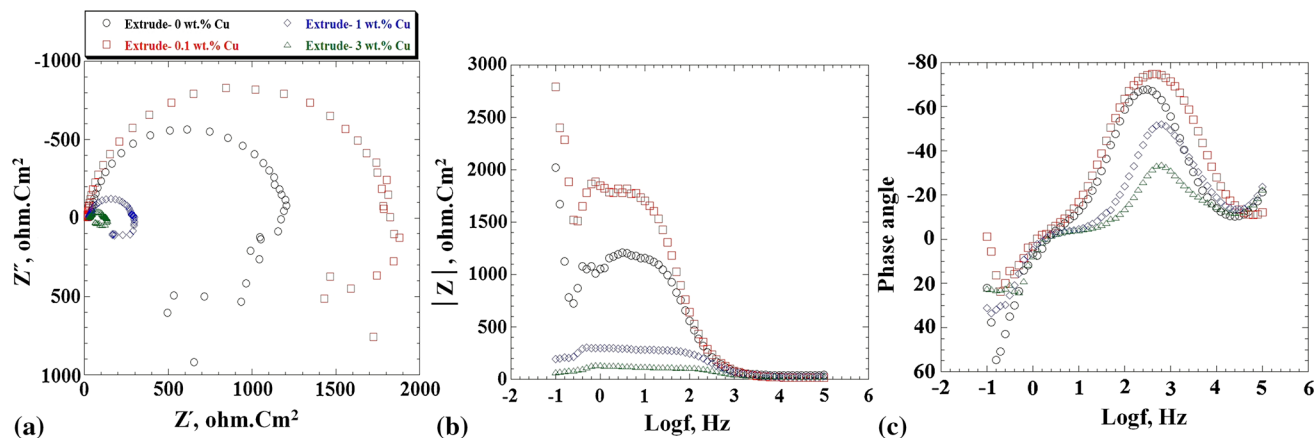


Fig. 13 EIS spectra of the extruded Mg-2%Zn-x%Cu alloys in 3.5 wt.% NaCl solution: (a) Nyquist plots; (b) Bode plots of $|Z|$ vs. frequency and (c) Bode plots of degree vs. frequency

Table 5 Values measured from the EIS curves of the cast and extruded Mg-2%Zn-x%Cu alloys after T6 treatments

Condition	Alloy	R_s	R_{ct}	R_f	R_L	L	C	C_f
Cast + T6	Mg-2%Zn	25.2 ± 1.3	755.1 ± 15.2	15.9 ± 1.2	$3.1E-8$	$3.1E-6$
	Mg-2%Zn-0.1%Cu	24.9 ± 0.9	946.4 ± 19.3	17.1 ± 1.1	49.3 ± 6.2	250.9 ± 9.9	$2.1E-8$	$2.5E-6$
	Mg-2%Zn-1%Cu	25.1 ± 0.2	178.5 ± 2.1	13.3 ± 1.2	79.2 ± 14.6	1817.9 ± 97.5	$3.8E-6$	$4.2E-6$
	Mg-2%Zn-3%Cu	24.1 ± 1.1	77.6 ± 1.6	9.3 ± 1.3	96.3 ± 12.5	6389.2 ± 102.4	$4.5E-6$	$6.5E-6$
Extrude + T6	Mg-2%Zn	26.9 ± 1.2	1190 ± 23.8	29.1 ± 2.5	47.9 ± 5.1	93.3 ± 4.7	$2.6E-8$	$2.9E-6$
	Mg-2%Zn-0.1%Cu	26.1 ± 0.4	1748 ± 28.9	31.3 ± 2.7	28.5 ± 5.2	77.8 ± 3.8	$1.5E-8$	$1.3E-6$
	Mg-2%Zn-1%Cu	25.6 ± 0.6	252.3 ± 4.4	16.4 ± 1.9	64.1 ± 9.9	302.5 ± 18.8	$2.4E-6$	$3.2E-6$
	Mg-2%Zn-3%Cu	25.4 ± 0.6	92.5 ± 1.6	13.1 ± 1.4	72.3 ± 10.3	4824.6 ± 112.2	$3.5E-6$	$5.1E-6$

low-frequency resistance and inductance. C is a constant phase element to report the non-homogeneity of the system ($R: \Omega \text{ m}^2$, $C: \mu\text{F cm}^{-2}$, $L: \text{H cm}^{-2}$) (Ref 21).

According to the fitting results from Table 5, it can be understood that the R_{ct} values arranged from the highest to the lowest as Mg-2%Zn-0.1%Cu ($946.4 \pm 19.3 \Omega \text{ cm}^2$), Mg-2%Zn ($755.1 \pm 15.2 \Omega \text{ cm}^2$), Mg-2%Zn-1%Cu ($178.5 \pm 2.1 \Omega \text{ cm}^2$) and Mg-2%Zn-5%Cu ($77.6 \pm 1.6 \Omega \text{ cm}^2$) for the cast alloys. For the extruded alloys, these sequence orders were as follows: Mg-2%Zn-0.1%Cu ($1748 \pm 28.9 \Omega \text{ cm}^2$), Mg-2%Zn ($1190 \pm 23.8 \Omega \text{ cm}^2$), Mg-2%Zn-1%Cu ($252.3 \pm 4.4 \Omega \text{ cm}^2$) and Mg-2%Zn-5%Cu ($92.5 \pm 1.6 \Omega \text{ cm}^2$). Generally, greater R_{ct} value represents the better corrosion resistance (Ref 21). Therefore, in this case, the T6 heat treatment after extrusion had a better response in comparison with the cast condition. Additionally, the cast and extruded Mg-2%Zn-0.1%Cu alloys showed the best corrosion resistance among other alloys. As can be seen, a minor addition of Cu (i.e., 0.1 wt.%) could progressively enhance the corrosion properties of the cast and extruded Mg-2%Zn alloy after the T6 heat treatment. Similar results were observed in previous work (Ref 19) that 0.1 wt.% Cu addition could improve the corrosion resistance of the cast Mg-2%Zn alloy. The reason was related to the volume fraction of the second-phase particles which acted as micro-cathodes for α -Mg phases (anodes) and accelerated the corrosion rate (Ref 19). The Mg-2%Zn-0.1%Cu alloy had the lowest Zn, Cu-containing intermetallics and finer grain structure among the other Cu-bearing alloys (Ref 19, 21). On the other hand, extrusion process changed the corrosion mechanism and

corrosion rate because of changing microstructure features like grain boundaries, the density of dislocations and twins and the distribution and rearrangement of second phases (Ref 22-24). Furthermore, in this work, the T6 heat treatment was led to enhancement of the corrosion resistance for the extruded alloys even more than that of the cast alloys. This can be related to three dominant factors: first, a more homogeneous microstructure with lower casting defects was achieved by extrusion process alongside with the T6 heat treatment. Second, double solution heat treatment was done before and after extrusion together with T6 heat treatment. More dissolution of second-phase intermetallics was achieved, and this phenomenon was led to less cathodic sites and better corrosion resistance. Third, by heat treatment process the amount of the grain boundaries, dislocations and twins reduced are considered as the other cathodic sites for α -Mg phases.

4. Conclusions

- (1) The microstructure has consisted of the α -Mg phase and two main intermetallics: MgZnCu and Mg(Zn,Cu)₂ phases. The solution and T6 heat treatments have been led to the formation of grain structure, incomplete dissolution of the intermetallics into α -Mg matrix and breakage of the continuous networks of second phases.
- (2) The grain size of the extruded alloys decreased with further Cu contents. Meanwhile, the T6 heat treatment in-

creased the grain size in comparison with the solution heat treatment. On the other hand, the volume fraction of intermetallics increased with more Cu additions and decreased a few with T6 heat treatment.

- (3) Further Cu additions and T6 heat treatment improved the Brinell hardness in both as-cast and hot-extruded conditions. The highest values of the Brinell hardness were achieved by 3 wt.% Cu addition and applying T6 heat treatment as 94 HBN and 116 HBN, respectively, for the as-cast and hot-extruded conditions.
- (4) The optimum level of UTS and elongation values obtained by 0.1 wt.% Cu addition for both cast and extruded alloys after solution and T6 heat treatments. The T6 heat treatment increased the UTS and decreased the elongation values in comparison with the solution heat treatment. By adding 3 wt.% Cu, the UTS and elongation values reduced for both cast and extruded alloys. Tensile strength (YTS) increased continuously with different Cu additions for the cast and extruded alloys after solution and aging heat treatments.
- (5) The cast and extruded Mg-2%Zn-0.1%Cu alloys presented more ductile fracture characteristics than the same cast and extruded alloys. Moreover, with more Cu additions, the extruded alloys had deeper and larger dimples than the cast alloys indicating better fracture mode. Furthermore, the volume fraction of the intermetallics inside the dimples increased with higher Cu additions.
- (6) The extruded alloys represented better corrosion resistance than the cast alloys. The extruded Mg-2%Zn-0.1%Cu alloy manifested the best corrosion resistance, due to more homogeneous microstructure resulted from hot extrusion and heat treatment. Also, higher Cu contents (> 0.1 wt.%) were led to more volume fractions of intermetallics and increased corrosion rates due to the extra cathodic sites.

References

1. D. Eliezer, E. Aghion, and F.H. Froes, Magnesium Science, Technology and Applications, *Adv. Perform. Mater.*, 1998, **5**, p 201–212
2. X. Gao and J.F. Nie, Characterization of Strengthening Precipitate Phases in a Mg-Zn Alloy, *Scr. Mater.*, 2007, **56**, p 645–648
3. J. Buha and T. Ohkubo, Natural Aging in Mg-Zn (-Cu) Alloys, *Metall. Mater. Trans.: A*, 2008, **39**, p 2259–2273
4. J.F. Nie, Precipitation and Hardening in Magnesium Alloys, *Metall. Mater. Trans.: A*, 2012, **43**, p 38919
5. R. Li, J. Nie, G. Huang, Y. Yin, and Q. Liu, Development of High-Strength Magnesium Alloys via Combined Processes of Extrusion, Rolling and Ageing, *Scr. Mater.*, 2011, **64**, p 950–953
6. X. Huang, A. Wu, Q. Li, and W. Huang, Effects of Extrusion and Ag, Zn Addition on the Age-Hardening Response and Microstructure of a Mg-7Sn Alloy, *Mater. Sci. Eng. A*, 2016, **661**, p 233–239
7. H.M. Zhu, G. Sha, J.W. Liu, C.L. Wu, C.P. Luo, Z.W. Liu, R.K. Zheng, and S.P. Ringer, Microstructure and Mechanical Properties of Mg-6Zn-xCu-0.6Zr (wt.%) Alloys, *J. Alloys. Comp.*, 2011, **509**, p 3526–3531
8. J. Buha, Reduced Temperature (22–100 °C) Ageing of an Mg-Zn Alloy, *Mater. Sci. Eng. A*, 2008, **492**, p 11–19
9. K. Ohishi, K. Hono, and K.S. Shin, Effect of Pre-aging and Al Addition on Age-Hardening and Microstructure in Mg-6wt.% Zn Alloys, *Mater. Sci. Eng. A*, 2008, **496**, p 425–433
10. B. Wang, F. Pan, X. Chen, W. Guo, and J. Mao, Microstructure and Mechanical Properties of As-Extruded and As-Aged Mg-Zn-Al-Sn Alloys, *Mater. Sci. Eng. A*, 2016, **656**, p 165–173
11. S. Zhu, T. Luo, T. Zhang, Y. Li, and Y. Yang, Effects of Cu Addition on the Microstructure and Mechanical Properties of As-Cast and Heat Treated Mg-6Zn-4Al Magnesium Alloy, *Mater. Sci. Eng. A*, 2017, **689**, p 203–211
12. F. Naghdi, R. Mahmudi, J.K. Kang, and H.S. Kim, Microstructure and High-Temperature Mechanical Properties of the Mg-4Zn-0.5Ca Alloy in the As-Cast and Aged Conditions, *Mater. Sci. Eng. A*, 2016, **649**, p 441–448
13. D.H. Ping, K. Hono, and J.F. Nie, Atom Probe Characterization of Plate-Like Precipitates in a Mg-RE-Zn-Zr Casting Alloy, *Scr. Mater.*, 2003, **48**, p 1017–1022
14. Y. Song, E.H. Han, D. Shan, C.D. Yim, and B.S. You, The Role of Second Phases in the Corrosion Behavior of Mg-5Zn Alloy, *Corros. Sci.*, 2012, **60**, p 238–245
15. H. Miao, H. Huang, Y. Shi, H. Zhang, J. Pei, and G. Yuan, Effects of solution treatment before extrusion on the microstructure, mechanical properties and corrosion of Mg-Zn-Gd alloy in vitro, *Corr. Sci.*, 2017, <http://dx.doi.org/10.1016/j.corsci.2017.01.001>
16. J. Lia, Q. Jiang, H. Sun, and Y. Li, Effect of Heat Treatment on Corrosion Behavior of AZ63 Magnesium Alloy in 3.5 wt.% Sodium Chloride Solution, *Corros. Sci.*, 2016, **111**, p 288–301
17. F. Cao, G.L. Song, and A. Atrens, Corrosion and Passivation of Magnesium Alloys, *Corros. Sci.*, 2016, **111**, p 835–845
18. S. Golmakaniyoon and R. Mahmudi, Comparison of the Effects of La- and Ce-Rich Rare Earth Additions on the Microstructure, Creep Resistance, and High-Temperature Mechanical Properties of Mg-6Zn-3Cu Cast Alloy, *Mater. Sci. Eng., A*, 2011, **528**, p 5228–5233
19. M. Lotfipour, M. Emamy, C. Dehghanian, and K. Tavighi, Influence of Cu Addition on the Structure, Mechanical and Corrosion Properties of Cast Mg-2%Zn Alloy, *J. Alloys. Comp.*, 2017, <http://dx.doi.org/10.1007/s11665-017-2672-0>
20. S.M. He, X.Q. Zeng, L.M. Peng, X. Gao, J.F. Nie, and W.J. Ding, Microstructure and Strengthening Mechanism of High Strength Mg-10Gd-2Y-0.5Zr Alloy, *J. Alloys. Comp.*, 2007, **427**, p 316–323
21. Y. Song, E.H. Han, D. Shan, C.D. Yim, and B.S. You, The Effect of Zn Concentration on the Corrosion Behavior of Mg-xZn Alloys, *Corros. Sci.*, 2012, **65**, p 322–330
22. T. Zhang, Y. Shao, G. Meng, Z. Cui, and F. Wang, Corrosion of Hot Extrusion AZ91 Magnesium Alloy: I-Relation Between the Microstructure and Corrosion Behavior, *Corros. Sci.*, 2011, **53**, p 1960–1968
23. N.N. Aung and W. Zhou, Effect of Grain Size and Twins on Corrosion Behaviour of AZ31B Magnesium Alloy, *Corros. Sci.*, 2010, **52**, p 589–594
24. G.L. Song and X.Z. Qing, The Surface, Microstructure and Corrosion of Magnesium Alloy AZ31 Sheet, *Elect. Acta*, 2010, **55**, p 4148–4161

Publisher's Note Springer Nature remains neutral with regard to jurisdictional claims in published maps and institutional affiliations.